

Scanned-slot digital mammography

Andrew D. A. Maidment, and Martin J. Yaffe

Departments of Medical Biophysics and Radiology, and the R.B. Holmes Radiological Research Institute,
University of Toronto, and the Physics Division, Ontario Cancer Institute,
500 Sherbourne St., Toronto, Ontario, Canada, M4X 1K9.

Abstract

A scanned-slot digital radiography system is being developed for use in mammography. The system consists of a novel fiber-optic "reformatter" which couples a strip of phosphor material to a light amplifier and a specially designed CCD camera. The reformatter provides an excellent means of converting a slot-shaped image to a format more suitable for digitization. A mammogram is produced by scanning the system in steps across the breast from the chest wall to the nipple. The pixels are of dimension $56\ \mu\text{m}$ by $49\ \mu\text{m}$ at the detector input. Images are currently acquired using a 40 kV tungsten anode spectrum with a measured half-value layer of 0.82 mm Al. The limiting resolution [MTF(f)=0.05] in the scanning direction is 9.2 cycles/mm. The quantum interaction efficiency of the phosphor is 64%, and the low-frequency detective quantum efficiency (DQE) was measured to be 0.60 ± 0.07 . The high-frequency DQE is superior to that of mammographic film-screen systems because of the ability to remove fixed-pattern noise from images. Phantom images produced with the scanned-slot system, and with a state-of-the-art film-screen mammography system were compared. The scanned-slot system demonstrated better contrast sensitivity using a lower mean glandular dose than the film-screen mammography system.

1. Introduction

In North America, approximately 1 in 10 women will develop breast cancer, and 1 in 20 women will die of the disease¹⁻⁴. It has been shown, however, that the risk of mortality can be reduced with early detection⁵⁻⁷. While film-screen mammography is the most sensitive and specific imaging modality currently available for the detection of breast cancer, previous work in our laboratory has shown that film-screen mammography systems suffer from three technical limitations^{8,9}. These relate to the compromise between image contrast and latitude caused by the shape of the characteristic curve of the film, the reduction of detective quantum efficiency (DQE) because of film granularity noise, and the dose inefficiency of conventional scatter removal techniques.

In previous work⁹ we developed an experimental scanned-slit digital mammography (SPDM) system to overcome the limitations of film-screen mammography, and were able to demonstrate improved contrast sensitivity. However, this slit system was not suitable for clinical use due to the limited x-ray quantum absorption efficiency of the detector, inappropriate detector geometry, and the long scan times required when using a single slit¹⁰.

An alternative and attractive approach to digital mammography is to acquire the data for all pixels simultaneously in a manner similar to film-screen imaging. Unfortunately, at this time, area detectors with the required spatial resolution, dynamic range, and noise properties are not available. We have, therefore, considered a scanned *slot* approach where multiple lines of the image are acquired simultaneously. In this configuration, a slot beam of x rays can be scanned across the breast, and the transmitted quanta are absorbed by a slot-shaped detector 2 to 5 mm wide. This configuration combined with both pre- and post-patient collimation provides scatter rejection two to three times better than that available with a mammographic grid¹⁰. To convert the unwieldy slot-shaped x-ray image to a format more suitable for digitization, while maintaining an adequate number of quanta at each stage of the imaging system, a custom fiber-optic reformatter (FOR) was designed. The FOR, illustrated in Figure 1, allows imaging very near the chest wall of the patient, which was not possible in the scanned-slit system. The FOR has a high transfer efficiency of light and excellent spatial resolution, thereby reducing possible degradation of the spatial-frequency dependent

detective quantum efficiency [DQE(f)]. We are currently developing a prototype scanned-slot digital mammography system (SSDM) based on a FOR, which can provide the improved imaging performance of the SPDM system, without the associated drawbacks.

2. System Description

2.1 System

The prototype SSDM system is shown schematically in Figure 2. The key element of the system, the FOR, consists of bundles of glass optical fibers arranged to form a rectangular slot-shaped input surface. In our experimental version, the input slot, of dimension 2 mm by 96 mm, is rearranged at the output to form eight 2 mm by 12 mm fiber bundles. A phosphor screen bonded to the input of the FOR absorbs the incoming x-ray beam and the resultant light passes through the FOR to form a scrambled optical image at the output surface. The scrambled image is then coupled to a specially-designed charge-coupled device (CCD) camera via a light amplifier (LA) and relay lenses. The LA is used to maintain adequate numbers of secondary quanta while allowing the image to be minified when coupled to the CCD. The output of the CCD is digitized to 12 bits, and transferred to a computer using direct memory access (DMA) techniques. The image is then unscrambled using a reconstruction algorithm. Multiple modules, consisting of a FOR, LA and CCD camera, can be butted together in the long dimension to image larger objects.

The x-ray generator is a 3-phase 12-pulse unit. Typically, images are acquired at 40 kVp (HVL = 0.82 mm Al). The detector is 60 cm from the focal spot. Currently, the object to be imaged is placed on a computer-controlled translation stage, and is scanned across the detector in steps. The pixel size at the detector is determined by the size of the CCD pixels and the magnification provided by the relay lenses. The CCD has pixels of dimension $19.75 \mu\text{m} \times 8.5 \mu\text{m}$, but the signals from every second pixel are summed to provide pixels which are nearly square. The relay lenses provide a magnification of 2.86 giving pixels of dimension $56 \mu\text{m}$ by $49 \mu\text{m}$ at the x-ray detector input, allowing 40 lines of an image to be acquired simultaneously.

A gantry is being developed to allow the imaging of patients. The lower surface of the breast will be placed on a support table which will be 55 cm from the focal spot. A 5 cm gap between the support table and the detector will allow the detector assembly to swing through an arc sufficient to image the entire breast, as illustrated in Figure 2. A

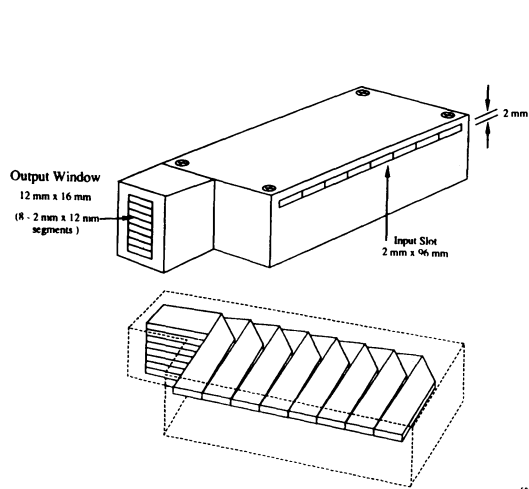


Figure 1. Detailed schematic of the fiber-optic reformatter (FOR).

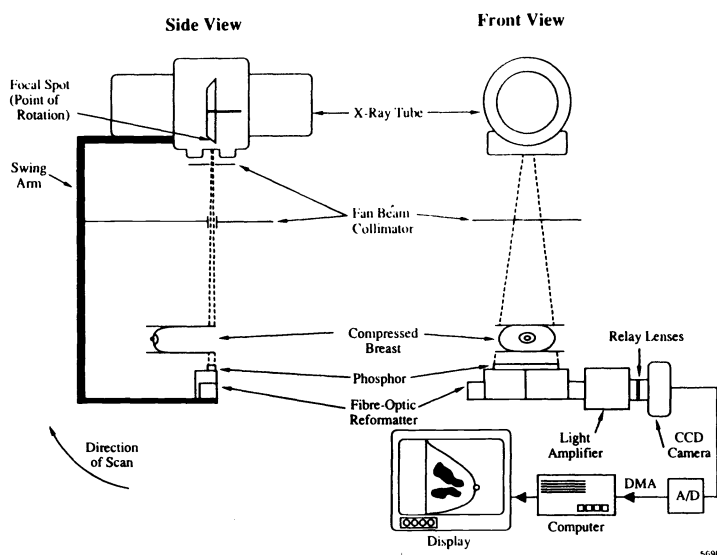


Figure 2. Schematic of the scanned-slot digital mammography system under development. Two FORs are shown to illustrate the ability to butt modules.

complete mammogram would be produced by scanning the system in steps across the breast from the chest wall to the nipple. Ninety slot images would be required to scan a distance of 18 cm.

2.2 CCD Camera

A dynamic range of greater than 2000 is required in digital mammography. This assumes that the maximum range of x-ray exposures through different parts of the breast⁹ is 400, and that the minimum signal-to-noise ratio required at the lowest exposure is 5. This wide dynamic range requirement necessitates that the CCD camera have extremely low noise levels. Because no commercially-available camera could meet our requirements, a camera was specially designed within our laboratory. The camera, shown schematically in Figure 3, has several features which aid in the reduction of noise. A virtual-phase frame-transfer CCD (Texas Instruments¹¹ TC 243) is used. The CCD uses on-chip correlated clamp sample-and-hold charge detection to reduce reset noise¹². Read noise is reduced with on-chip integration of charge, and slow readout (one fifth standard video rates, i.e. 2.86 megasamples per second). As shown in Figure 3, the output of the CCD is divided into three channels, which are digitized individually. This allows reduction of the readout speed by an additional factor of three. The analog-to-digital converters (ADCs) are connected to an optional summing circuit, which provides a means of summing every second pixel of the CCD, producing an effective CCD pixel of dimension 19.75 μm by 17.0 μm . The output of the summing circuit is sent to one of two FIFO registers. While one register is being used to accumulate one line of the image, the second is being emptied using a burst-mode DMA transfer procedure.

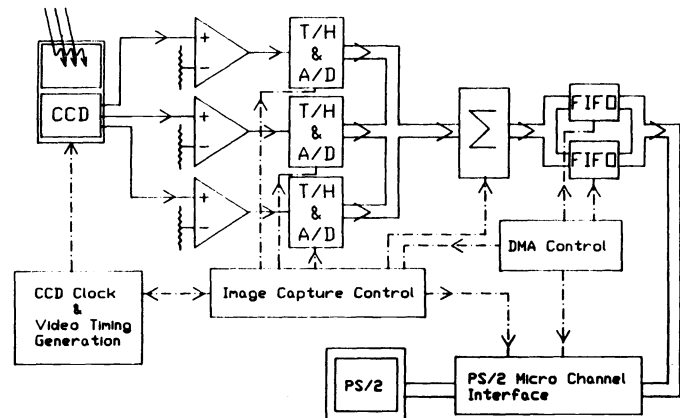


Figure 3. Schematic of the CCD camera, showing the three channel architecture, summing circuit (Σ), and DMA interface.

To correct for temperature-dependent variations in offset voltage, as well as to reduce thermally-generated electrons, two Peltier effect coolers were bonded to the CCD chip. When operated at -2.5°C thermal dark noise and non-thermal read noise are of comparable magnitude.

2.3 Image Reconstruction

Images generated by the SSDM system are composed of many 2 mm by 96 mm slot sub-images. Each sub-image is composed of eight 2 mm by 12 mm segments which are rearranged by the FOR as shown in Figure 1. Several steps are performed in sequence to reconstruct the final slot-shaped sub-image from the constituent segments. Many slot sub-images are then assembled into a mosaic that forms the final mammogram. Figure 4 shows a single digitized (scrambled) 2 mm wide slot sub-image of a star resolution test pattern. The image contains 7 of the 8 segments of the FOR. Figure 5 shows a reconstructed image of this star pattern produced using the technique described below.

In the reconstruction, the output data are first corrected for the non-linearity of the CCD chip. The linearity measurement is discussed in Section 3.1.2. The non-linearity is the result of the design of the charge-detection stage of the CCD. The charge is detected through a reverse-biased diode¹³, hence the capacitance of this detection node is proportional to the charge in the node. The result is a non-linearity in converting charge to voltage. Since there is a one-to-one relationship between the intensity of light incident on the CCD and its signal, an inverse relationship can be calculated, and is used to produce a look-up table of the corrections to be applied to each pixel in the image.

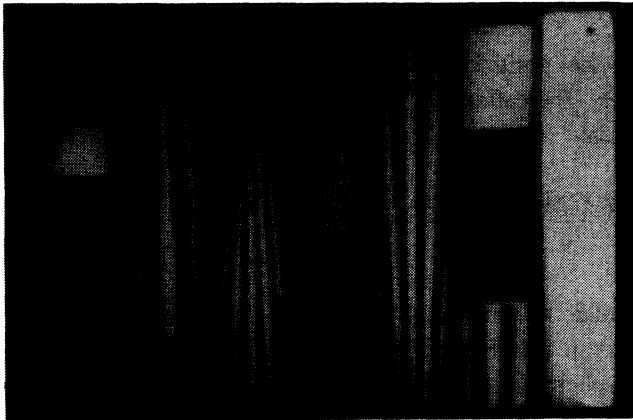


Figure 4. A slot sub-image prior to reformatting.

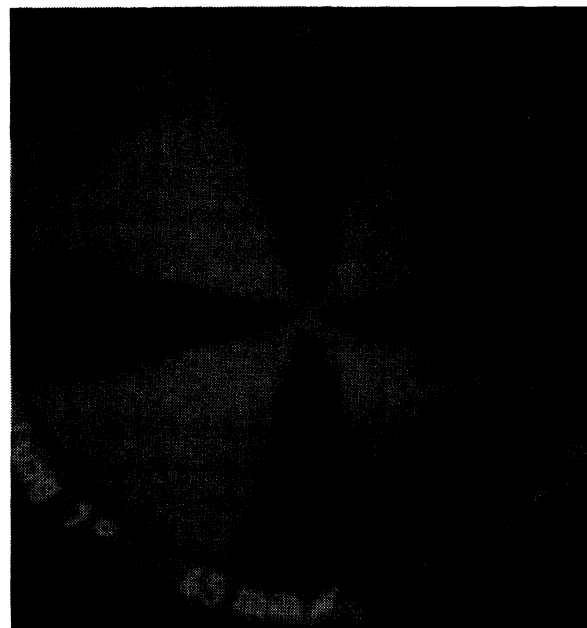


Figure 5. A reconstructed image of a radiographic star pattern.

Next, the temporally invariant noise of the imaging system [also called structural, or fixed-pattern noise (FPN)] is removed from each slot sub-image. This correction allows for the removal of pixel-to-pixel sensitivity and offset variations. The corrected signal, S'_{IJ} , for pixel IJ is given by

$$S'_{IJ} = \frac{S_{IJ} - D_{IJ}}{B_{IJ} - D_{IJ}} \times (\bar{B} - \bar{D}) \quad , \quad (1)$$

where S_{IJ} is the measured pixel value, B_{IJ} is a measurement of the pixel at high illumination (approximately 3/4 of saturation), and D_{IJ} is a measurement of the pixel with no illumination. To eliminate the effects of x-ray quantum noise on B_{IJ} , and dark noise on D_{IJ} , many images were averaged. \bar{B} is the mean signal (averaged spatially) of the high illumination image, and \bar{D} is the mean signal (averaged spatially) of the zero illumination image. The effectiveness of this correction is illustrated in Figure 6, which is a histogram of pixel values for irradiation of the system at a level yielding a signal about two thirds of \bar{B} . Results are shown before and after correction for pixel-to-pixel variations. The full width half-maximum of the corrected histogram is 0.3% of the mean.

The third step in the correction process is necessary to remove the pin-cushion distortion introduced by the LA. The edges of each segment of the FOR are straight, hence any observed deviation from a straight line can be used to generate a correction function. A quadratic curve is fitted to the edge of each segment of the image of the FOR, and the fit is used to calculate the distortion for each row of pixels in each segment. These offsets are used to remove the distortion from each segment, row by row, using linear interpolation.

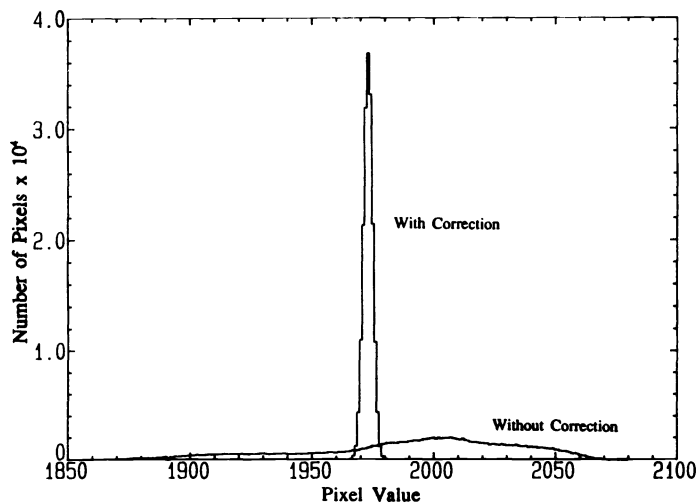


Figure 6. Histogram of CCD response to uniform illumination with and without corrections for pixel-to-pixel sensitivity and offset variations.

Next, a correction is applied to remove misalignments due to variations in the angle at which each fiber-optic segment is bonded to its neighbour at the input slot and output window. Since the variations are small (less than 3°), linear interpolation is used to correct for these alignment errors. Finally, each segment of the FOR image is transferred to the composite image which forms the mammogram.

Each of the corrections described above is independent of the position of the slot with respect to the patient, therefore it is necessary to formulate these corrections only once. Thereafter, the correction procedure may be applied automatically to each slot sub-image acquired by the SSDM system.

3. Characterization of Components

3.1 CCD Camera

The CCD camera has been evaluated in terms of signal-to-noise, linearity, and resolution. All measurements were performed with a specially designed light source¹⁴ consisting of an integrating light sphere, and green light-emitting diodes whose spectral emission is similar to that of the P20 phosphor of the LA.

3.1.1 Mean-Variance

For a system where the generation of signal carriers is governed by Poisson statistics, it can be shown^{15,16} that

$$\sigma_s^2 = \bar{G} \cdot \bar{S} + \sigma_{\text{READ}}^2, \quad (2)$$

where \bar{G} is the mean conversion gain in analog-to-digital conversion units (ADU) per signal carrier (electron), \bar{S} is the observed mean signal in ADU, σ_s^2 is the observed variance in ADU², and σ_{READ}^2 is the square of the signal-independent or "read" noise in ADU².

The points in a plot of the mean and variance for various illuminations should fall along a straight line whose slope is \bar{G} , and whose intercept with the ordinate is σ_{READ}^2 . Results of such an experiment with our CCD camera are shown in Figure 7. A least-squares fit generated a slope corresponding to $\bar{G} = 0.0385 \pm 0.0003$ ADU/e, i.e. 26.0 electrons per ADU. From the known gain of the amplifiers, and the calibration of the ADCs, we calculated the responsivity of the CCD to be 4.18 ± 0.03 $\mu\text{V}/\text{e}$, which was in agreement with the manufacturer's specification. From the intercept of the fit, σ_{READ} was calculated to be 1.6 ± 0.2 ADU. This corresponds to $\sigma_{\text{READ}}/\bar{G} = 42 \pm 6$ electrons. The measured noise for zero illumination was 22 ± 2 electrons. The nature of this discrepancy is being investigated.

The mean-variance technique provides an excellent means of calculating the saturation signal of the CCD. Saturation has occurred when the measured variance begins to roll off at high illuminations. This is the result of the sharing of charge between adjacent pixels on the CCD which reduces the variance. We have measured the point of departure from the fit in previous experiments. The amplification used, was chosen to set the signal at saturation (S_{SAT}) to 3950 ADU. This corresponds to a well capacity of 1.03×10^5 electrons. The dynamic range of the CCD, defined as the ratio of maximum signal to minimum noise ($S_{\text{SAT}}/\sigma_{\text{READ}}$), was calculated using the fitted value of the read noise to be 2500.

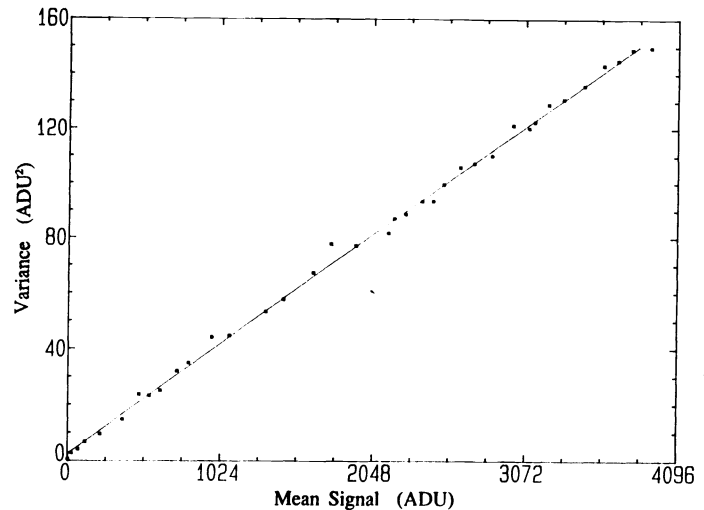


Figure 7. Mean-variance analysis of the CCD camera.

3.1.2 Linearity

It was found that the response of the CCD as a function of illumination could be fitted to the power law

$$\bar{S} = C \cdot I^\gamma + D, \quad (3)$$

where \bar{S} is the signal in ADU, C converts illumination to ADUs, γ is the power of the fit, and D is an offset to account for the signal at zero illumination. A fit was made to minimize a root-mean-square (RMS) distance parameter. For illumination varying from zero to CCD saturation (15 ADU to 3950 ADU), the best fit of γ was 0.958. The RMS variation of the data points about the fitted curve was 0.89 ADU. This relationship was used to calculate a look-up table to correct for the non-linearity of the CCD. The look-up table was constructed to match the corrected and uncorrected signal values at zero illumination and CCD saturation. This will lead to the largest corrections being applied to mid-range values. The correction for a signal of 2000 ADU is -63 ADU or -3.2%.

3.1.3 Resolution

The modulation transfer function (MTF) was determined from measurement of the edge spread function (ESF). A razor blade was placed at the focal plane of the relay lenses at about a 2° angle with respect to either the rows or columns of the CCD. The blade obscured about one half of the sensitive area of the CCD. The resultant image consists of a set of ESFs, each displaced slightly with respect to the next. Using the method of Judy¹⁷, the ESFs were combined to yield an oversampled edge. This edge was numerically differentiated to obtain the line spread function (LSF), and the Fourier transform of the normalized LSF was calculated to obtain the MTF. The MTFs of the CCD camera and relay lenses in the x- and y-direction are shown in Figure 8. The CCD response is non-isoplanatic since its pixels are rectangular. Adjacent pixels were not summed in this experiment.

3.2 Light Amplifier

The use of a LA introduces concerns about a non-linear response to illumination and the formation of a secondary quantum sink at the photocathode of the LA. The linearity of the LA was measured in a similar fashion to that of the CCD camera. A plot of linearity of the LA over 5 orders of magnitude of illumination is shown in Figure 9. Illumination of the LA was varied using the variable intensity light source and neutral density filters. Here, the CCD camera served as a radiometer, and was coupled to the output of the LA via variable aperture relay lenses to prevent CCD saturation. The RMS variation from a linear least-squares fit between illumination and output was less than

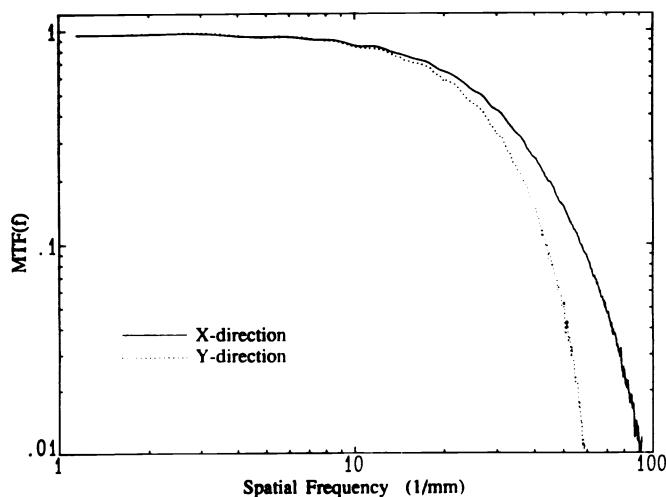


Figure 8. MTF of the CCD camera and relay lenses in the x- and y-direction.

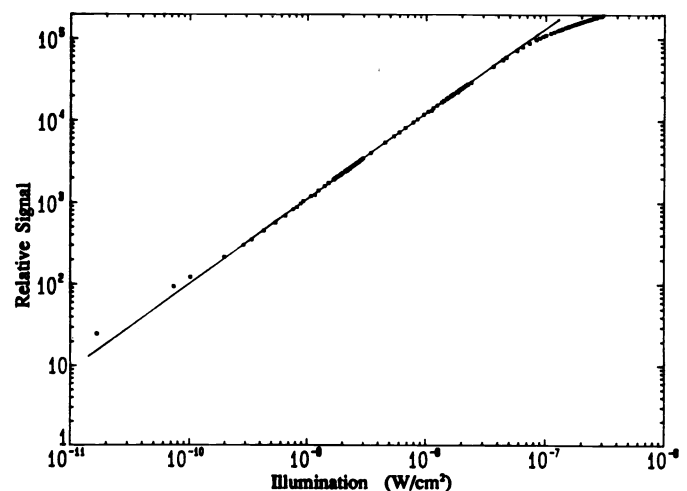


Figure 9. Linearity of the light amplifier.

1 per cent for illuminations between 1.8×10^{10} W/cm² and 6.0×10^8 W/cm². At higher illumination, automatic brightness controls, which prevent damage to the LA, introduced a non-linearity. At low illumination, the dark current of the radiometer added a bias to the measurement. The concern of the formation of a secondary quantum sink is addressed in Section 4.2.

4. System Evaluation

4.1 Resolution

The resolution of the system was measured using the technique described in Section 3.1.3. The MTFs of the components are shown in Figure 10. The MTF of the CCD camera and relay lenses is represented by the dotted curve. Here, the MTF was calculated with adjacent pixels summed in the x-direction, and has been presented in terms of the spatial frequencies at the plane of the input slot. The MTF including the effect of the LA is represented by the dashed curve. The solid curve represents the MTF of the system with x-ray irradiation using a Kodak Min-R intensifying screen as the phosphor element of the detector. A slanted 0.4 mm thick tantalum plate with a knife-edge was used to obscure one half of the image field. The limiting resolution [i.e. $MTF(f)=0.05$] was measured to be 9.2 cycles/mm. This is in good agreement with artifact-free regions of Figure 5. The MTF of the SSDM system is compared to film-screen mammography systems and our previous work^{9,18} in Figure 11.

4.2 Quantum Accounting

The mean number of quanta measured at each stage in the imaging system (labelled A through J in Figure 12), per x-ray quantum incident on the detector, is presented in Figure 13. The fraction of x-ray quanta which interact with the phosphor is 0.64 (N_p/N_x). Assuming an effective energy of 22 keV, approximately 400 light photons (N_c/N_p) will be produced, of which 45 percent (N_e/N_c) will illuminate the photocathode of the LA. It is estimated, given the efficiency of the photocathode, and the spectrum of the incident light, that on average $N_e/N_p = 10.3$ photoelectrons are emitted per x-ray photon interaction. The LA provides an optical gain of 520 (N_p/N_e), which is sufficient to allow coupling of the LA to the CCD with $f/2.0$ relay lenses. The result is that for one x-ray photon interaction, 370 light photons (N_c/N_p) are incident on the CCD, generating $N_e/N_p = 165$ electrons. The digitized value then, is $N_e/N_p = 6.4$ ADU per x-ray interaction.

For our preliminary work, the relay lenses were used to provide adjustable minification of the image, allowing control of the resolution and the field of view of the detector. In part, the minification was necessary to match the

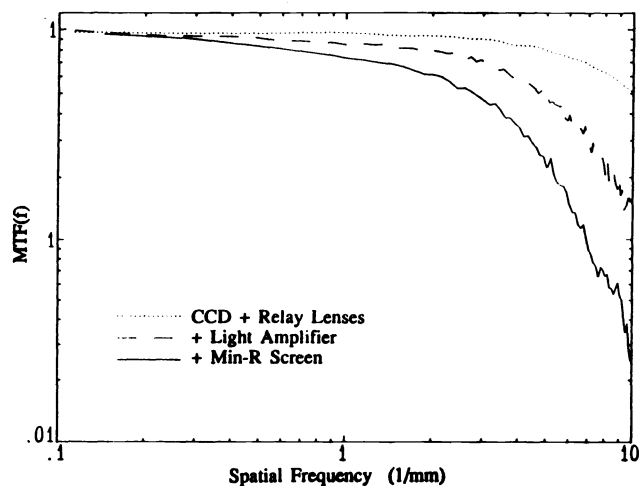


Figure 10. MTF(f) of the SSDM system and components.

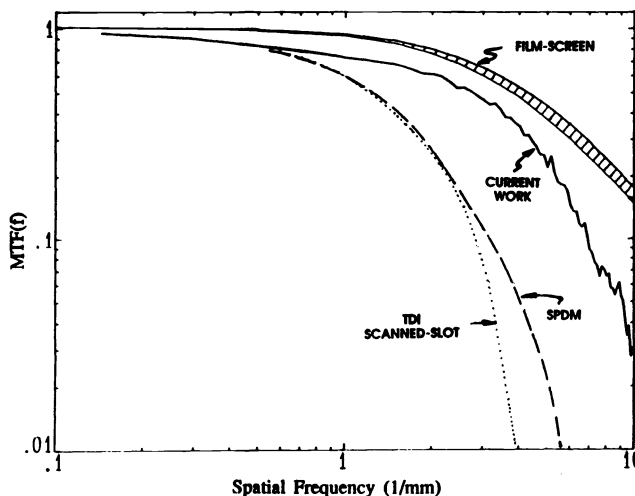
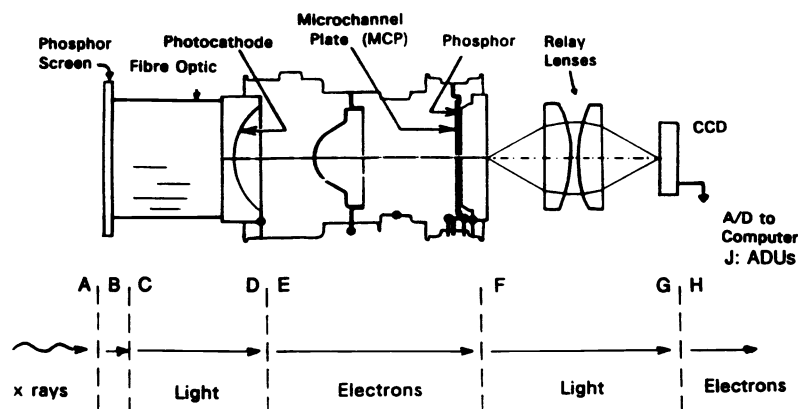
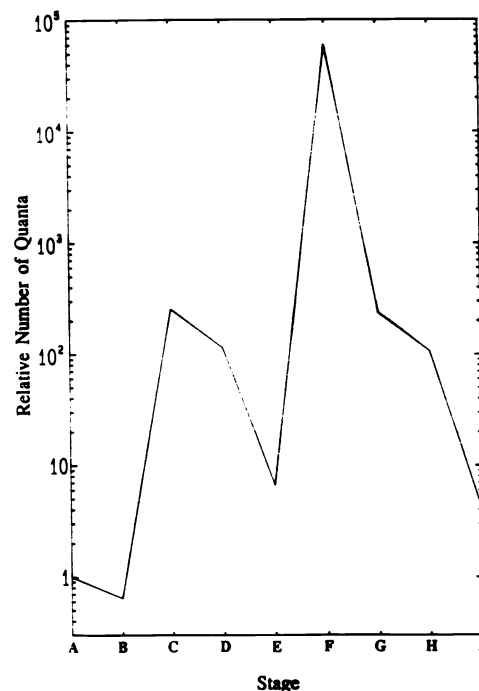


Figure 11. MTF(f) of the SSDM system, our previous SPDM⁹ and TDI¹⁸ systems, and several film-screen mammography systems.



(↑) Figure 12. Schematic illustrating the stages where the number of quanta was measured.

(→) Figure 13. Number of quanta at each stage (N_{STAGE}).



12 mm x 16 mm FOR output to the 4.8 mm x 6.3 mm CCD. The LA was required to avoid a quantum sink at H, due to the 0.4% efficiency of the lens optics and the 45% quantum efficiency of the CCD. The LA, however, was found to saturate at the upper end of the required range of signals and, therefore, restricted the x-ray fluence rates that could be used for imaging. We are now investigating direct fiber-optic coupling of the FOR to a larger CCD of dimension 12.0 mm x 12.2 mm, which would allow elimination of the LA and the relay lenses. The removal of the intensity restriction will permit reduced scan time.

4.3 Detective Quantum Efficiency

To analyze the signal-to-noise performance of the SSDM system, the total system noise power spectrum [$W_T(f)$] with uniform x-ray irradiation was measured. Fixed-pattern noise was removed from the images and a correction for the non-linearity of the CCD was performed prior to calculating $W_T(f)$. A synthesized slit⁹ 0.05 mm wide and 3.36 mm long was used. $W_T(f)$ was calculated by averaging the individual power spectra from several images. The MTF(f) and $W_T(f)$ data were combined to calculate DQE(f) using⁹,

$$DQE(f) = \frac{\Phi \cdot [K \cdot MTF(f)]^2}{W_T(f)} \quad (4)$$

where Φ is the x-ray fluence at the detector, and K is a constant that allows expression of the detector output in terms of fluence (at zero spatial frequency). The

calculated DQE(f) is shown in Figure 14. Also shown are the DQEs of the SPDM system described in Section 1, a system using a time-delay integration (TDI) type CCD camera coupled to an experimental beryllium window x-ray image intensifier⁸, and several commercially available film-screen mammography systems⁹. Referring to Figure 11, it can be seen that the MTF of the SSDM system exceeds that of the two previous digital systems, but is inferior to the

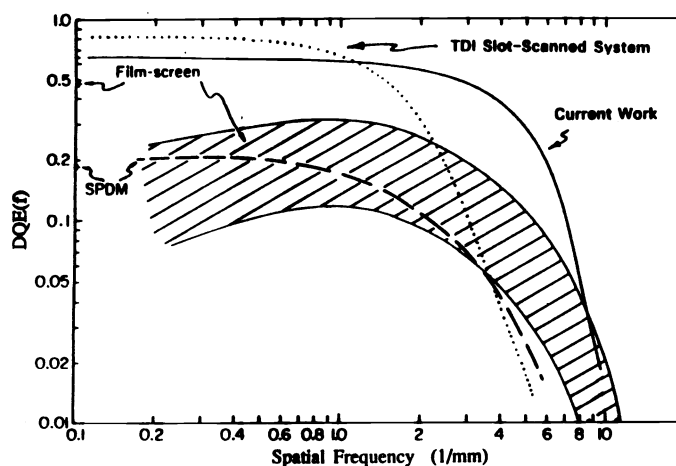


Figure 14. DQE(f) of the SSDM system, our previous SPDM⁹ and TDI⁸ systems, and several film-screen mammography systems.

film-screen systems. Nevertheless, the $DQE(f)$ of the SSDM system exceeds that of all film-screen systems up to about 9 cycles/mm. This is due to the low read noise of the CCD camera, and the ability to remove FPN. The SSDM system also exceeds the performance of the SPD system, but has an inferior $DQE(f)$ to the TDI system at low spatial frequencies, because of the excellent scintillation efficiency of the x-ray detector in the TDI system¹⁸.

4.4 Contrast-Detail Perceptibility

To determine the potential improvement in the detection of breast lesions, we evaluated the prototype SSDM system with a contrast-detail phantom. The phantom is a 4.0 cm thick block of lucite with a 0.8 cm thick overlay consisting of stacked Mylar sheets with holes ranging in diameter from 0.12 mm to 7.53 mm, and ranging in depth from 0.13 mm to 3.05 mm. Images of this phantom were acquired with both the SSDM system, and a state-of-the-art film-screen mammography system. The SSDM image was acquired with a dose to the phantom equivalent to a mean glandular dose of 0.05 cGy. The film-screen image was obtained with a Kodak ortho-M/Min-R system, using a 30-kVp molybdenum spectrum filtered by 0.051 mm of molybdenum, with a dose to the phantom equivalent to a mean glandular dose of 0.08 cGy. The digital image had a format of 3,000 by 1500 pixels, over which the user could "pan" and "zoom" at will within a 1024x1024 pixel frame, as shown in Figure 15. A contrast-detail perceptibility curve showing the median of the results of four readers is given in Figure 16. The subject contrast was calculated for the x-ray spectrum and scatter conditions that applied to the film-screen system. In spite of the reduced scatter, the subject contrast at the input to the SSDM system was about 20% less than that of the film-screen system, due to the higher energy spectrum used. Clearly, the SSDM system enables better low-contrast object detection. At higher contrast, the improvement is less dramatic. This is due to image artifacts. In this preliminary study, several small high-contrast objects fell along the joints between FOR segments. The artifacts in these images must be removed prior to a complete assessment of the system's performance.

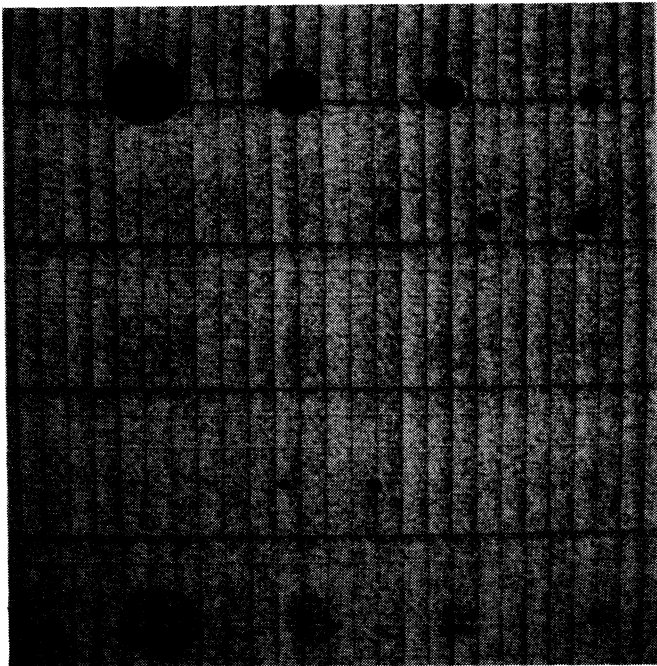


Figure 15. A 1024 x 1024 pixel section of an image obtained with the SSDM system, of the contrast-detail phantom.

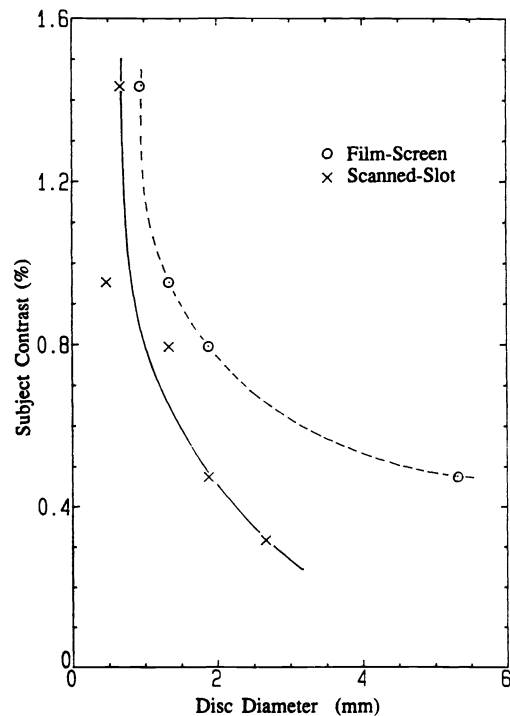


Figure 16. Contrast-detail perceptibility curve for the SSDM system, and a state-of-the-art film-screen mammography system.

5. Summary

We have designed and constructed a prototype scanned-slot digital radiography system with the resolution and contrast sensitivity required for use in mammography. To maximize DQE(f), we have attempted to create a system where noise is dominated by x-ray quantum fluctuations. This was achieved with: a) the use of the fiber-optic reformatter, which provides efficient coupling of the slot-shaped input image to the CCD; b) the very low read noise and excellent dynamic range of the CCD camera; and, c) the removal of fixed-pattern noise. We have demonstrated that the SSDM system has DQE(f) and contrast sensitivity superior to that of a state-of-the-art film-screen mammography system. Currently, the images obtained with the SSDM system contain unacceptable artifacts that are the result of the manufacture of the FOR, and the reconstruction software. These artifacts must be removed prior to use in a clinical setting. We are investigating a number of ways of eliminating these artifacts.

6. Acknowledgements

We are grateful to Brian Starkoski, N. Robert Bennett, and Gordon E. Mawdsley for their assistance. The generosity of GE-CGR (France), Kodak Canada Inc., and Synergistic Detectors Inc. (Mountain View, CA) in providing equipment to further this project is greatly appreciated. Financial assistance was provided by The National Cancer Institute of Canada, The Medical Research Council of Canada, and The Ontario Cancer Treatment and Research Foundation. The first author is supported by an Ontario Graduate Scholarship.

7. References

1. Cancer Facts and Figures - 1987, American Cancer Society, New York, 1987.
2. Cancer in Canada - 1983, Statistics Canada, Ottawa, 1988.
3. Cancer in Ontario - 1987, The Ontario Cancer Treatment and Research Foundation, Toronto, 1988.
4. Canadian Cancer Statistics - 1988, Canadian Cancer Society, Toronto, 1988.
5. P. Strax, L. Venet, and S. Shapiro, "Value of mammography in reduction of mortality from breast cancer in mass screening", AJR, 117(3), 686-689, 1973.
6. S. Shapiro, *et al.*, "Ten- to fourteen-year effect of screening on breast cancer mortality", JNCI, 69(2), 349-355, 1982.
7. L. Tabar, *et al.*, "Reduction in mortality from breast cancer after mass screening with mammography", Lancet i, 829-832, 13 April 1985.
8. R.M. Nishikawa, and M.J. Yaffe, "Signal-to-noise properties of mammographic film-screen systems", Med. Phys., 12(1), 32-39, 1985.
9. R.M. Nishikawa, G.E. Mawdsley, A. Fenster, and M.J. Yaffe, "Scanned-projection digital mammography", Med. Phys., 14(5), 717-727, 1987.
10. M.J. Yaffe, R.M. Nishikawa, A.D.A. Maidment, and A. Fenster, "Development of a digital mammography system", In: Medical Imaging II: Part I - Image Formation, Detection, Processing and Interpretation, R.H. Schneider, and S.J. Dwyer III, Editors, Proc. SPIE 914, 182-188, 1988.
11. Texas Instruments Inc., P.O. Box 655012, Dallas, Texas, 75265.
12. J. Hyncek, "High-Resolution 8-mm CCD Image Sensor with Correlated Clamp Sample and Hold Detection Circuit", IEEE Trans. Electron Dev., ED-33(6), 850-862, 1986.
13. J. Hyncek, "Design and Performance of a Low-Noise Charge-Detection Amplifier for VPCCD Devices", IEEE Trans Electron Dev., ED-31(12), 1713-1719, 1984.
14. J. A. Rowlands, K. S. Schulenburg, and G. DeCrescenzo, "A light source for testing radiological television cameras", Med. Phys., 16(1), 1-6, 1989.
15. L. Mortara, and A. Fowler, "Evaluations of charge-coupled device (CCD) performance for astronomical use", In: Solid State Imagers for Astronomy, J.C. Geary, and D.W. Latham, Editors, Proc SPIE 290, 28-33, 1981.

16. G.R. Sims, and M.B. Denton, "Characterization of a charge-injection-device camera system as a multichannel spectroscopic detector", Opt. Eng., **26**(10), 1008-1019, 1987.
17. P.F. Judy, "The line spread function and modulation transfer function of a computed tomographic scanner", Med. Phys., **3**(4), 233-236, 1976.
18. D.W. Holdsworth, R.M. Nishikawa, G.E. Mawdsley, M.J. Yaffe, and A. Fenster, "Slot-beam digital mammography using a time-delay integration (TDI) CCD", In: Medical Imaging III: Image Formation, R.H. Schneider, S.J. Dwyer III, and R.G. Jost, Editors, Proc. SPIE **1090**, 306-313, 1989.